Climate Dynamics (1999) 15:937–951 

M. Todd · R. Washington

# Circulation anomalies associated with tropical-temperate troughs in southern Africa and the south west Indian Ocean

Received: 11 August 1998 / Accepted: 28 May 1999

**Abstract** Daily rainfall variability over southern Africa (SA) and the southwest Indian Ocean (SWIO) during the austral summer months has recently been described objectively for the first time, using newly derived satellite products. The principle mode of variability in all months is a dipole structure with bands of rainfall orientated northwest to southeast across the region. These represent the location of cloud bands associated with tropical temperate troughs (TTT). This study objectively identifies major TTT events during November to February, and on the basis of composites of NCEP reanalysis data describes the associated atmospheric structure. The two phases of the rainfall dipole are associated with markedly contrasting circulation patterns. There are also pronounced intra-seasonal variations. In early summer the position of the temperate trough and TTT cloud band alternates between the SWIO and southwest Atlantic. In late summer the major TTT axis lies preferentially over the SWIO, associated with an eastward displacement in the Indian Ocean high. In all months, positive events, in which the TTT cloud band lies primarily over the SWIO, are associated with large-scale moisture flux anomalies, in which convergent fluxes form a pronounced poleward flux along the cloud band. This suggests that TTT events are a major mechanism of poleward transfer of energy and momentum. Moisture transport occurs along three principle paths: (1) the northern or central Indian Ocean (where anomalous fluxes extend eastward to the Maritime Continent), (2) south equatorial Africa and the equatorial Atlantic, (3) from the south within a cyclonic flow around the tropical-temperate trough. The relative importance of (2) is greatest in late summer. Thus, synoptic scale TTT events over SA/SWIO often result from large-scale planetary circulation patterns. Hovmoeller plots show that TTT development coincides with enhanced tropical convection between 10°–30 °E (itself exhibiting periodicity of around 5 days), and often with convergence of eastward and westward propagating convection around 40 °E. Harmonic analysis of 200 hPa geopotential anomalies show that TTT features are forced by a specific zonally asymmetric wave pattern, with wave 5 dominant or significant in all months except February when quasi-stationary waves 1, 2 and 3 dominate. These findings illustrate the importance of tropical and extratropical dynamics in understanding TTT events. Finally, it is suggested that in November–January TTT rainfall over SA/SWIO may be in phase with similar rainfall dipole structures observed in the South Pacific and South Atlantic convergence zones.

M. Todd (✉) · R. Washington
School of Geography, University of Oxford,
Oxford OX1 3TB, UK
E-mail: martin.todd@geog.ox.ac.uk

## 1 Introduction

The nature of rainfall variability over southern Africa (SA) has been investigated on numerous time scales, including the synoptic (Harrison 1986), though interannual (Jury et al. 1992; Jury 1997; Nicholson and Kim 1997; Rocha and Simmonds 1997) to decadal and millennial (Tyson 1986; Cohen and Tyson 1995; Stokes et al. 1997). Focus on southern Africa is driven in part by the importance of rain-fed agriculture to the economy of the region, and the observed high degree of interannual variability in rainfall. Perhaps for this reason, and owing due to the absence of accurate estimates of rainfall over the surrounding ocean areas, analysis of rainfall over the southwest Indian Ocean (SWIO) has been limited. The impact of this rainfall on the atmospheric structure of the region has therefore been overlooked. It is known that a significant proportion of summer rainfall is derived from tropical-temperate troughs (TTTs) which extend over both continental

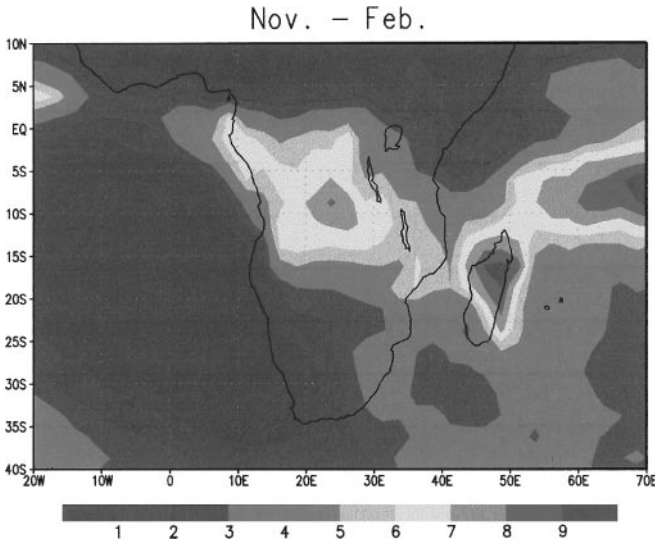


**Fig. 1** Mean rain rate (mm day$^{-1}$) for summer months November–February (1979–1995)

SA and the adjacent SWIO (Harrison 1984, 1986; Todd and Washington 1998; Washington and Todd 1999). It follows that studies of the atmospheric signals related to land-based rainfall should consider the SA/SWIO region as a whole.

During TTT events a band of cloud and rain links tropical convection with transients in the midlatitudes. SA and the SWIO is one of three known preferred locations for such tropical-temperate interaction in the Southern Hemisphere (Streten 1973). Unlike its counterparts, namely the South Atlantic and South Pacific convergence zones (SACZ and SPCZ, respectively), the SA/SWIO feature is not semi-permanent and exists only during the austral summer months. Rainfall associated with TTTs is reflected in the mean field of monthly summer rainfall (Fig. 1), in this case derived from a combination of satellite infrared and passive microwave measurements, rain gauge observations and numerical modelled fields (Xie and Arkin 1997). Peak summer rainfall is associated with the ITCZ and occurs over central SA at about 10 °S and eastward over the Indian Ocean. Another band of rainfall associated with TTTs extends south and east from central Africa extending to the midlatitudes over the SWIO at about 60 °E.

Whilst the dynamical mechanisms of these TTT features remain poorly understood, variability in the location and frequency of occurrence of the SWIO cloud band has important implications for rainfall over South Africa. In a synoptic classification of central southern African rainfall, Harrison (1984, 1986) shows that TTTs represent the single most significant rain-producing system type.

Todd and Washington (1998) and Washington and Todd (1999) used empirical orthogonal functions (EOFs) (see Sect. 2.2) of satellite-derived estimates of daily rainfall (see Sect. 2.2) to determine the dominant modes of daily summer rainfall variability over SA and the SWIO. In each austral summer month (November–March), with the exception of February, the principle mode of daily rainfall variability is a dipole structure characterised by two opposing rain bands oriented northwest to southeast across southern Africa and the SWIO, representing the location of TTT features (Fig. 2). Numerical modelling experiments have also suggests a dipole in the preferred location of TTT systems (vanden Heever et al. 1997). During February, a single tropical-temperate rain band links southeast southern Africa with the southwest Indian Ocean. Instead of the land-based convection centred over southern Africa linking with temperate rainfall systems, convection over Zambia, Zimbabwe and Western Angola link with convection over the subtropical Indian Ocean and the associated tropical-temperate trough. Rainfall over much of South Africa in February is not directly associated with this interaction.

Thus, although TTTs emerge as the leading mode of daily rainfall variability, there is monthly variability in their structure and location. Events characterised by such tropical-temperate connections occur relatively infrequently and with marked interannual variability. Average rainfall anomalies (over 2.5° grid cells) associated with composites of the major extreme temperate-tropical events peak at 8–10 mm day$^{-1}$ in each month. The proportional contribution of these small number of extreme events to total rainfall is substantial and tends to be highest over ocean regions (in all months exceeding 65% over the Mocambique channel), confirming the dominant role of TTT in summer rainfall over the study region.

Other work has identified a similar dipole structure in rainfall over the region at longer interannual scales which has been related to the preferred location of a trough-ridge system in the monthly mean pressure field in the region (Jury et al. 1992). Todd and Washington (1998) suggest that the position of this structure can vary on much shorter time scales. The significance of tropical temperate troughs over SA and SWIO in the transfer of energy, momentum and moisture between tropical and temperate latitudes has been analysed by Harrison (1984, 1986), D'Abreton and Lindesay (1993), D'Abreton and Tyson (1995).

Using the objective definition of TTT events of Todd and Washington (1998) and Washington and Todd (1999), in combination with recently released global reanalysis data, this study presents an analysis of the structure of the regional and global atmosphere associated with the distinct phases of the TTT rainfall dipole. In doing so we seek to provide an explanation of the spatial pattern of TTT rainfall and its intraseasonal variability.

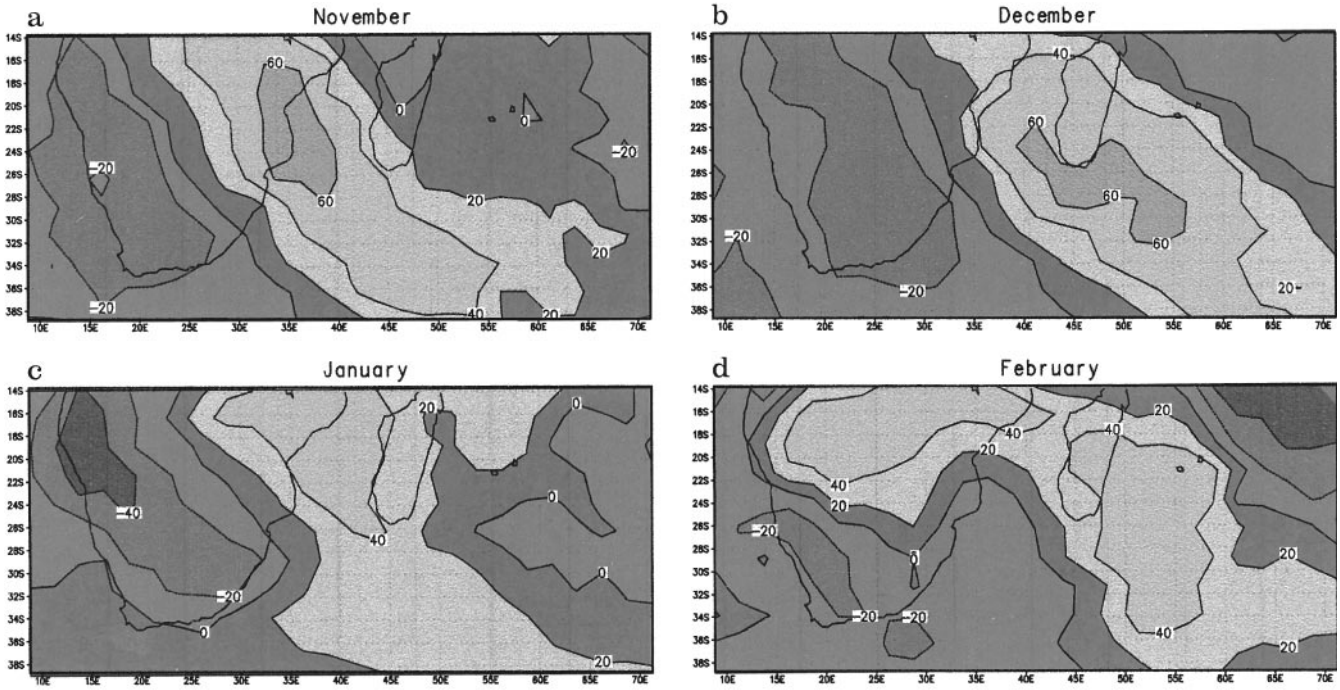


**Fig. 2a–d** EOF 1 weights of daily rainfall for: **a** November, **b** December, **c** January, **d** February (from Todd and Washington 1998)

## 2 Data and methodology

### 2.1 Data

Todd and Washington (1999) describe a technique to retrieve 3 h estimates of global tropical and subtropical (40 °N–40 °S) rainfall at 2.5° resolution from satellite infrared observations contained within International Satellite Cloud Climatology Program (ISCCP) D1 data (Rossow and Schiffer 1991). Although the ISCCP D1 data set is currently incomplete, it will ultimately extend from 1983 to present. The method entails a reconstruction of the GOES Precipitation Index (GPI) (Arkin and Meisner 1987), and the products are hereafter referred to as the reconstructed GPI (RGPI). Although RGPI estimates of rainfall exhibit minimal bias with respect to the GPI, it is thought that the GPI, which was calibrated using oceanic data from the Global Atmospheric Research Program (GARP) Atlantic Tropical Experiment (GATE), may have a tendency to overestimate land-based convective rainfall totals (Kidd and Adler 1997). The 3-h resolution of the RGPI products contrasts with rainfall estimates based on measurements of outgoing longwave radiation (OLR) from polar-orbiting satellites which provide samples at best twice per day (for periods where only one satellite is in operation). The RGPI therefore represent the most extensive set of global tropical and subtropical rainfall products available for continental and oceanic regions, with the high temporal frequency necessary for analysis of rainfall features at the daily and sub-daily scale.

Daily rainfall was derived using the RGPI algorithm on a 2.5° grid for the austral summer months of November through February (listed in Table 1), covering the period 1986–93 inclusive. In order to study the structure of the atmosphere, 12-h global analyses were obtained for these months on a 2.5° grid from the NCEP-NCAR reanalysis project (Kalnay et al. 1996). Data from three levels (850, 500 and 200 hPa) were used in this study to represent low, mid and upper tropospheric conditions. An evaluation of forecast products and moisture transport in the NCEP model can be found in Mo and Higgins (1996).

### 2.2 Methods

The study domain for analysis of daily RGPI rainfall estimates covers a region of SA and the SWIO bounded by latitudes 15° to 40° South (the maximum southerly extent of RGPI rainfall estimates) and longitudes 7.5° to 70° East. Todd and Washington (1998) and Washington and Todd (1999) conducted EOF analysis on daily rainfall for each of the austral summer months. Table 2 presents the eigenvalue proportions of the first five unrotated EOFs of the correlation matrix, and the North test (North et al., 1992) results of eigenvalue separation. The leading EOFs of daily rainfall for individual months are shown in Fig. 2 as the correlation coefficients between the daily rainfall time series at each of the grid boxes and the EOF time coefficients (scores). The EOF time coefficients are the cross product of the eigenvectors and the standardised daily rainfall time series. The study region was selected after a number of experiments on the sensitivity of EOF analysis to domain size, shape and location had been conducted so that the EOF solutions presented are not contingent upon a priori decisions (see Washington and Todd 1999 for a complete description).

The results of this work for November through to February were used to identify extreme events characteristic of tropical-temperate troughs objectively. From the EOF time coefficients (explained already) the major extreme positive (negative) events typical of the leading EOF in each month are objectively identified by extracting days with coefficients above (below) one standard deviation from the mean (Fig. 3). These episodes represent the major events associated with the centres of activity of the TTT rainfall dipole structure (Todd and Washington 1998). Table 1 presents the dates of the positive and negative extreme events used in the analysis.

Positive events account for a larger portion of the rainfall variance than negative events over eastern SA and the SWIO. It should be noted that whilst the EOF loading patterns are dominated by TTT rainfall structure, the dipole pattern and location of the TTT is variable through the austral summer season. During January, rainfall associated with negative events is truncated at the south coast of SA, in February the dipole structure is absent. In

**Table 1** Dates of daily data used to form composites of positive and negative TTT events

| | November | | December | | January | | February | |
|---|---|---|---|---|---|---|---|---|
| | Positive | Negative | Positive | Negative | Positive | Negative | Positive | Negative |
| 1986 | 9,28 | | 9–14,22,23,30,31 | | 1,5–9 | 19–21,26,27 | 6–10 | 3 |
| 1987 | — | — | — | — | 1–5, 23–26 | | — | — |
| 1989 | 4,10,16,27–30 | | 3,18–20 | | — | — | — | — |
| 1990 | 24,25 | 7,8,27 | | 1,4,5,15 | 1–3 | 22–28 | 7,11 | 3,4,19,28 |
| 1991 | 14–16,20–22 | 4–8,10,27 | 5 | 3,7,8,14,17–20,28 | 10,11 | 15–18,20–26 | 10,14–17 | |
| 1992 | 17,25 | | 24–27 | | | 8,9 | | 8–13,18–22,28 |
| 1993 | — | — | — | — | 11–20 | | 2,8,11–16,22–25 | |

**Table 2** Variance of monthly EOFs and sampling errors based on North test (North et al. 1982)/ = pass x = fail

| EOF | November Variance | $n = 150$ North | December Variance | $n = 155$ North | January Variance | $n = 186$ North | February Variance | $n = 141$ North |
|---|---|---|---|---|---|---|---|---|
| 1 | 8.54 | 0.34 / | 9.41 | 0.35 / | 11.78 | 0.36 / | 8.37 | 0.34 / |
| 2 | 6.78 | 0.21 / | 7.93 | 0.32 / | 10.99 | 0.34 / | 6.52 | 0.30 / |
| 3 | 5.84 | 0.28 / | 5.46 | 0.27 / | 6.85 | 0.27 / | 5.42 | 0.28 / |
| 4 | 5.11 | 0.26 / | 5.00 | 0.25 x | 6.13 | 0.25 / | 4.52 | 0.25 / |
| 5 | 4.67 | | 4.80 | | —– | | 4.10 | |

these months negative events are not strictly representative of TTT events.

These events form the basis of composites of positive and negative episodes for which the mean anomalies of global RGPI rainfall and of NCEP reanalysis atmospheric fields were calculated. In subsequent diagrams shaded areas represent the regions where the composite mean anomalies are statistically significant at the 5% level (based on a *t*-test).

Moisture flux at a given level (g $g^{-1}$-$ms^{-1}$) in the zonal ($Q_u$) and meridonal ($Q_v$) planes can be calculated from:

$$Q_u = qu \tag{1}$$

$$Q_v = qv \tag{2}$$

where $q$ is specific humidity (g $g^{-1}$) and $u$ and $v$ and the zonal and meridonal wind components respectively.

Numerous studies have shown that rainfall over SA/SWIO is modulated by the Southern Oscillation (Lindesay et al. 1986; Janowiak 1988; Ropelewski and Halpert 1989; Nicholson and Kim 1997). In a study of this kind, it is possible that systematic differences between the circulation patterns associated with positive and negative events, may primarily reflect inter-annual variability, such that positive or negative events, may occur predominantly in ENSO warm or cold phases. In such a condition the rainfall dipole pattern would be driven by interannual rather than synoptic scale variability. To test whether this is the case, all the study months were classified as El Nino or La Nina events, on the basis of the monthly Southern Oscillation Index. Then, for each of the four study months separately, the data used in composite analysis were tested for sampling bias using a 2-sample $\chi^2$ test on the frequency of occurrence of El Nino and La Nina conditions in positive versus negative events. In all months except February there is no significant difference between positive and negative events in terms of their respective sampling of El Nino and La Nina conditions. Thus, any differences between patterns of rainfall and atmospheric structure associated with positive and negative events are unlikely to be due to sampling bias, although the database as a whole, originating as it is from recent years, includes a preponderance of El Nino events. In February, however, the sampling of the negative events is significantly biased toward El Nino events.

## 3 Structure of the atmosphere associated with tropical temperate troughs in Southern Africa and the Southwest Indian Ocean

### 3.1 Early summer

The rainfall EOF structure in the early summer months of November and December is remarkably similar, differing only in the detail of the TTT location. These months are therefore discussed together.

During November positive events, significant 850 hPa geopotential composite anomalies are negative (peaking at −30 gpm) along the axis of the TTT (Fig. 4). Negative anomalies are also found over Africa east of 20 °E, extending into the western and central Indian Ocean north of 15 °S. Significant positive departures occur west of the southern African subcontinent centred on 35 °S and 10 °E. An anomalous ridge of near surface high pressure, peaking at 30 gpm near 45 °S and 75 °E is also apparent. December 850 hPa geopotential composite anomalies for positive events (not shown) are similar, except that the trough described is located slightly eastward and there is less structure in the mid-latitude anomaly field. Negative event composites of 850 hPa geopotential (Fig. 4) are in most respects the reverse of the positive events, particularly south of 15 °S. During these events a weak tropical low is located over western SA, and the Indian Ocean subtropical high lies close to the mean position, extending over eastern SA. The Atlantic high is displaced northwest allowing a weak temperate trough to lie to the southwest of SA. Poleward flow results over SA with a cloud band oriented from western SA across the continent along the TTT. Thus the

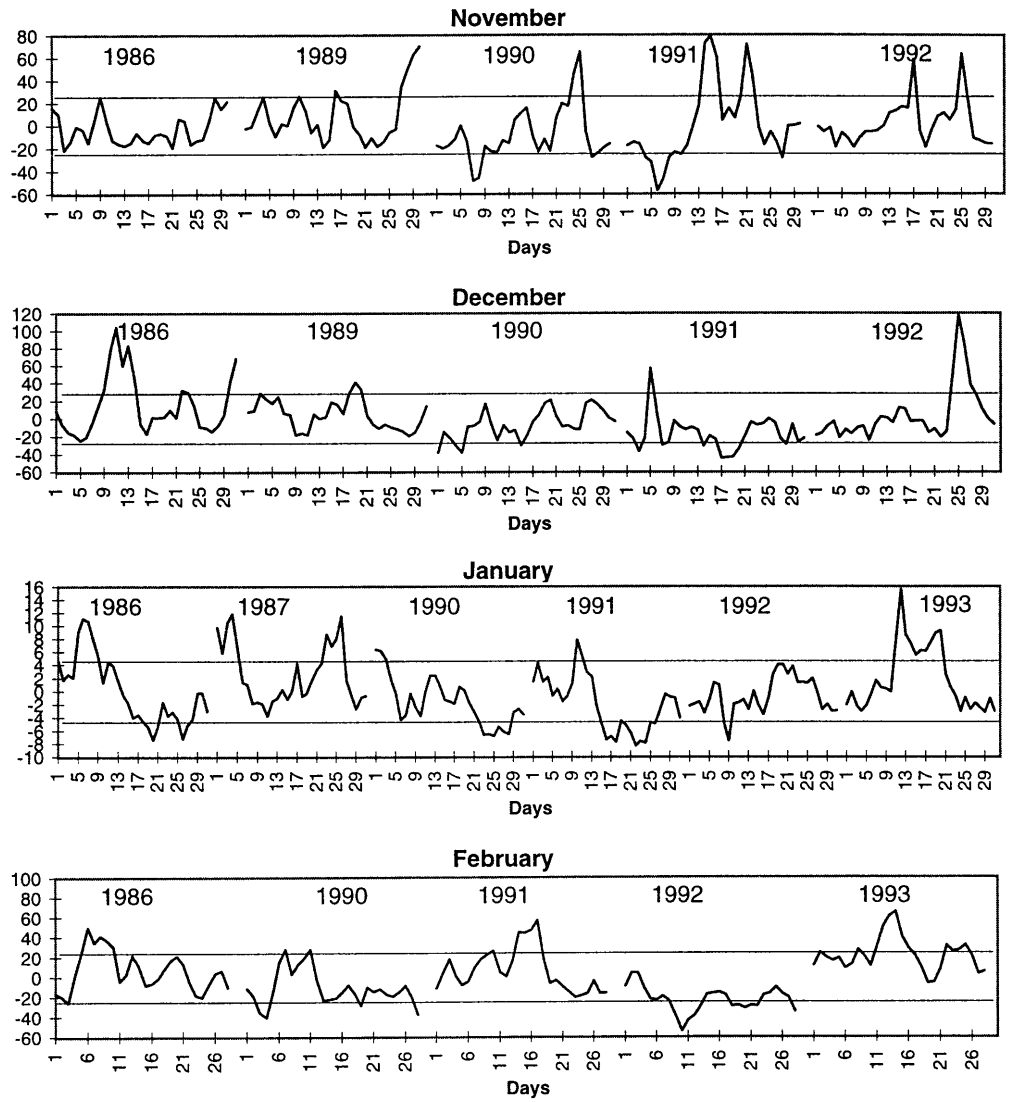


**Fig. 3a–d** Time coefficients of EOF 1 (with ±1 standard deviation shown): **a** November, **b** December, **c** January, **d** February (from Todd and Washington 1998)

early summer TTT structure shows an east-west alternation in position between the SWIO and southwest Atlantic.

An important feature of the early summer near surface pressure field structure is a ridge, trough, ridge (trough, ridge, trough) structure in the case of positive (negative) events. At 200 hPa, the geopotential anomalies are of the same sign as the surface anomalies (Fig. 5) but with the ridge, trough, ridge system west leaning, indicating a baroclinic atmosphere.

Table 3 shows the variance and amplitudes of the zonal harmonic waves at 200 hPa for composite positive and negative events at 45 °S. In November positive events the zonally asymmetric circulation in the upper troposphere is dominated by wave 5 which accounts for just under 40% of the variance and has an amplitude of 36 gpm. The trough of this wave overlies southern Africa. Wave 5 is also important during December, although transient waves 4 and 6 all explain similar variance. The most significant feature of December, however, lies in the variance associated with standing wave 1.

Low-level (850 hPa) moisture flux composites for November positive and negative events are shown in Fig. 6. There are three main paths of anomalous moisture flux for positive events, namely:

1. A northerly flux from the Northern Indian Ocean
2. A north westerly flux from equatorial southern Africa and the far eastern equatorial Atlantic
3. A southerly cyclonic flow around the tropical-temperate trough

Convergence of these three moisture conduits occurs in the Mocambique Channel near 20 °S. Southward moisture flux occurs between 10 °N and at least 40 °S, while a remarkably coherent zonal near surface flux occurs between 120 °E and 45 °E centred on 5 °N. It is clear that the anomalous moisture flux associated with early summer TTTs, with convergence over the Mocambique Channel, occurs at a planetary scale, marking TTTs as major events in the general circulation of the atmosphere. Inspection of 500 hPa moisture flux anomalies (Fig. 6) shows that the anomalous

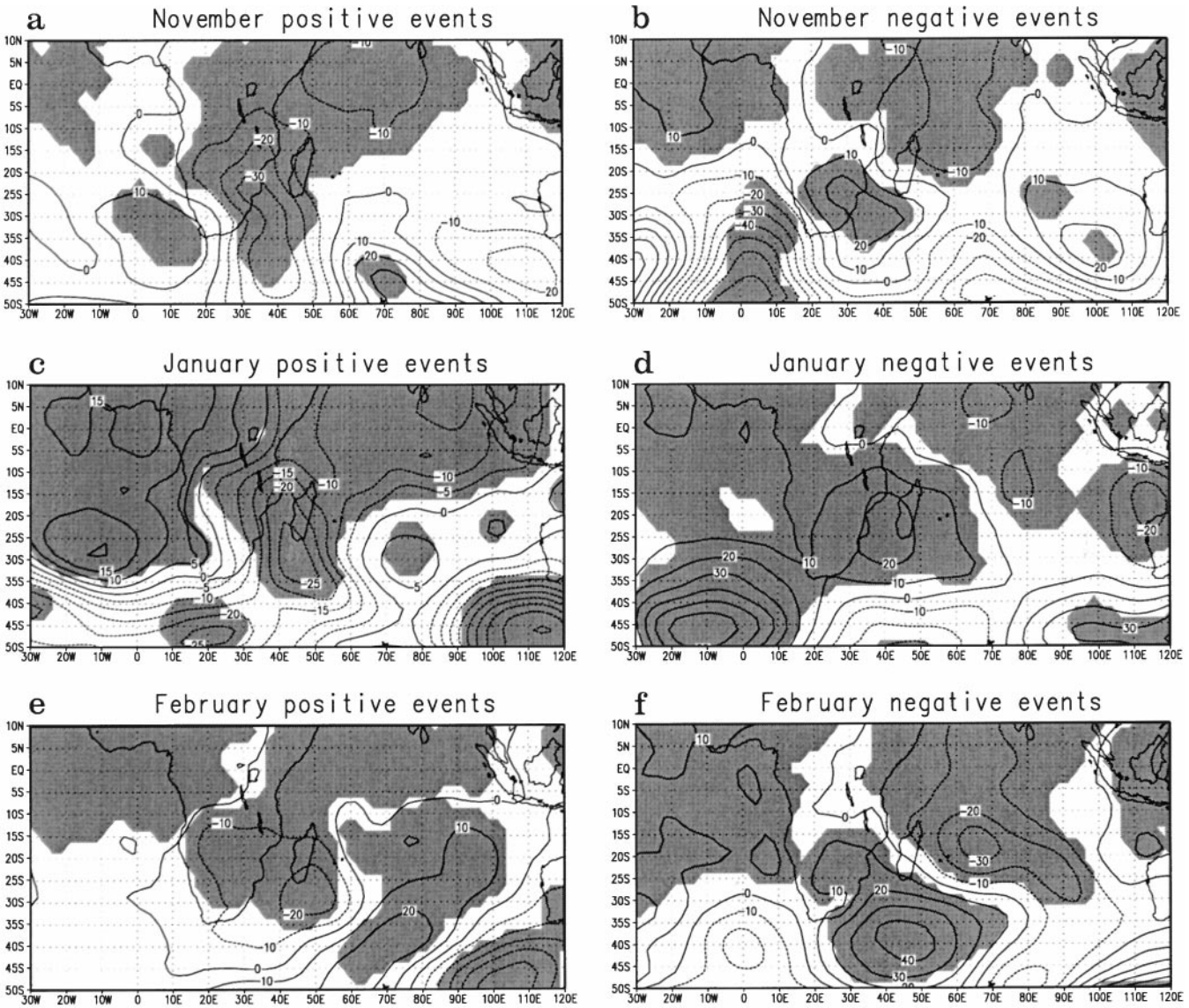


**Fig. 4a–f** Composite mean 850 hPa geopotential height anomalies (gpm) for **a** November positive events, **b** November negative events, **c** January positive events, **d** January negative events, **e** February positive events, **f** February negative events. *Shaded areas* are statistically significant at 95% level

equatorial flux extends at least 5 km into the atmosphere. At this height, moisture from tropical convection near 10 °S 30 °E also serves as an important source with a southward flux of moisture extending from 5 °S to at least 50 °S overlying the TTT cloud band.

Early summer negative events are characterised by a less uniform structure, with low level moisture flux from the Atlantic being more important for these events. Poleward low level flux of moisture occurs near 20 °E and 80 °E. December moisture flux composites (not shown) are strikingly similar to November cases, except that the vectors are generally smaller and the westward low level conveyor across the Northern Indian Ocean during positive events occurs south of the equator centred on 5 °S during December.

The evolution of TTTs may be studied by means of Hovmoeller plots of composite rainfall anomalies. Figure 7 shows the time evolution of this field 10 days prior to, and 5 days after the start of the TTT events, for four latitude bands (0°–10 °S, 10°–20 °S, 20–30 °S, 30°–40 °S), over the domain 20 °W to 120 °E. Tropical convection between 20 °E and 30 °E in the latitudinal band 0°–10 °S shows a pulsing of enhanced and suppressed convective activity at 5-day intervals. Rainfall anomalies propagate towards the east. In addition, rainfall pulses, occurring at least 10 days prior to the main TTT event near 80 °E, appear to propagate towards the west, forming a convergence of positive rainfall anomalies at the TTT event. Eastward propagation is evident in rainfall anomalies at latitude bands

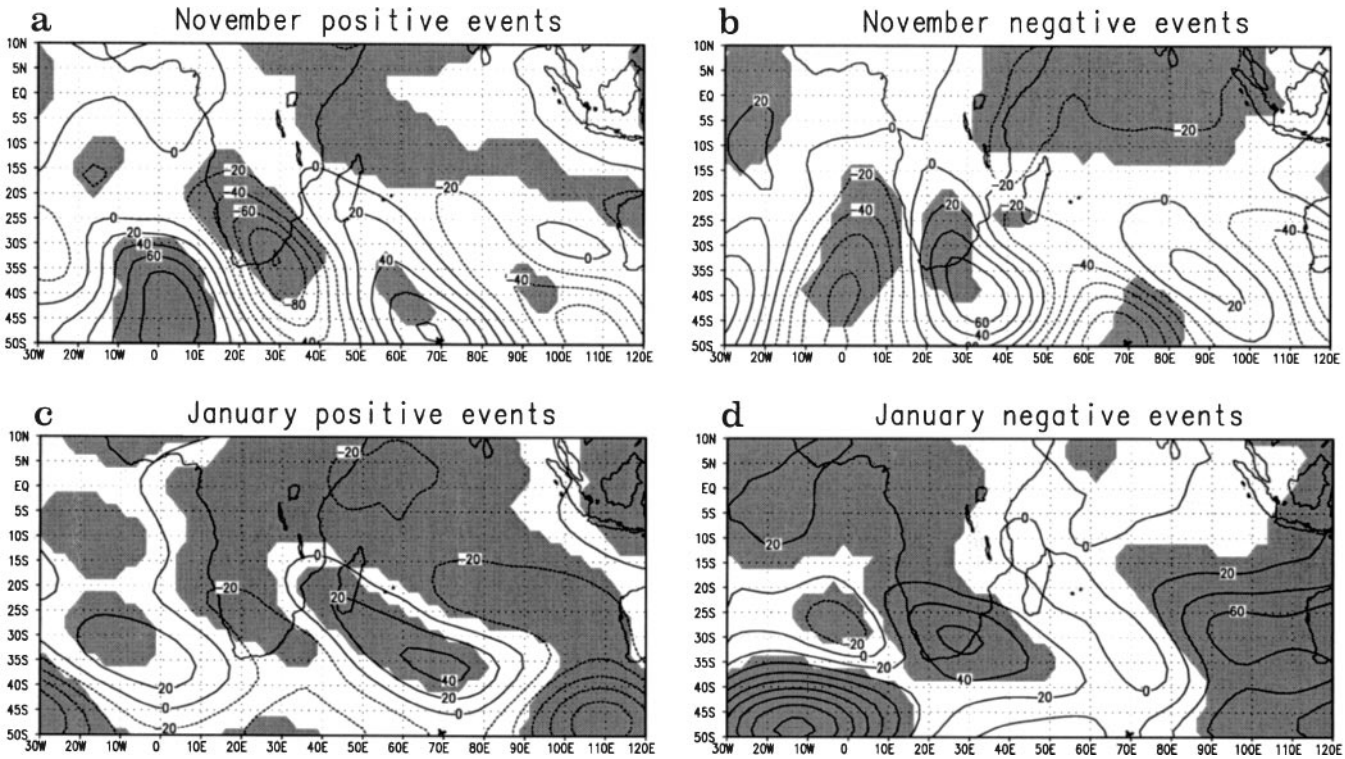


**Fig. 5a–d** Composite mean 200 hPa geopotential height anomalies (gpm) for **a** November positive events, **b** November negative events, **c** January positive events, **d** January negative events. *Shaded areas* are statistically significant at 95% level

**Table 3** Amplitude and variance of first 10 harmonics (most important 3 in bold) of composite mean 200 hPa geopotential anomalies (gpm) for positive events at 45 °S

| | 1 | 2 | 3 | 4 | 5 | 6 | 7 | 8 | 9 | 10 |
|---|---|---|---|---|---|---|---|---|---|---|
| November | | | | | | | | | | |
| Amplitude | **24.7** | 14.2 | 10.1 | 13.9 | **35.9** | **22.6** | 14.4 | 9.8 | 5.5 | 1.7 |
| Variance | **18.6** | 6.2 | 3.7 | 5.9 | **39.5** | **15.6** | 6.4 | 2.9 | 0.9 | 0.1 |
| December | | | | | | | | | | |
| Amplitude | **36.9** | 18.7 | 18.3 | **26.1** | **23.1** | **25.7** | 10.7 | 6.5 | 3.3 | 1.7 |
| Variance | **33.2** | 8.6 | 8.2 | **16.6** | **12.9** | **16.1** | 2.8 | 1.0 | 0.3 | 0.1 |
| January | | | | | | | | | | |
| Amplitude | 11.4 | 0.9 | 19.7 | **16.9** | **37.3** | 6.7 | 6.6 | 3.4 | 0.4 | 3.0 |
| Variance | 5.3 | 0.0 | 16.8 | **12.4** | **60.5** | 1.9 | 1.9 | 0.5 | 0.0 | 0.4 |
| February | | | | | | | | | | |
| Amplitude | **23.8** | **29.2** | **31.3** | 13.0 | 8.9 | 5.5 | 4.2 | 8.9 | 6.2 | 2.4 |
| Variance | **19.9** | **30.2** | **34.7** | 5.9 | 2.8 | 1.0 | 0.6 | 2.8 | 1.3 | 0.2 |

centred on 15°, 25° and 35 °S. Much smaller, eastward propagating positive rainfall anomalies are apparent in the 30°–40 °S panel some 5 days prior to the TTT event. It is tempting to speculate that these episodes failed to be realised as TTT events because of a concomitant convective break in tropical convection evidenced by the negative rainfall anomalies at this time near 5 °S, 25 °E.

### 3.2 Late summer

There are important differences in the structure of the leading rainfall modes which constitute the late summer months. January and February are therefore discussed separately.

The January circulation patterns associated with positive and negative events, inferred from the mean composite of the low level (850 hPa) and upper level (200 hPa) geopotential fields are shown in Figs. 4 and 5. During positive events, a statistically significant anomalous near surface TTT is located to the east of SA, extending from around 10 °S to at least 50 °S. This feature is associated with an eastward retreat of the Indian Ocean subtropical high, but negative departures extend over the entire Indian Ocean north of about 10 °S. Positive departures are found over much of the tropical Atlantic. A deep trough is also located near

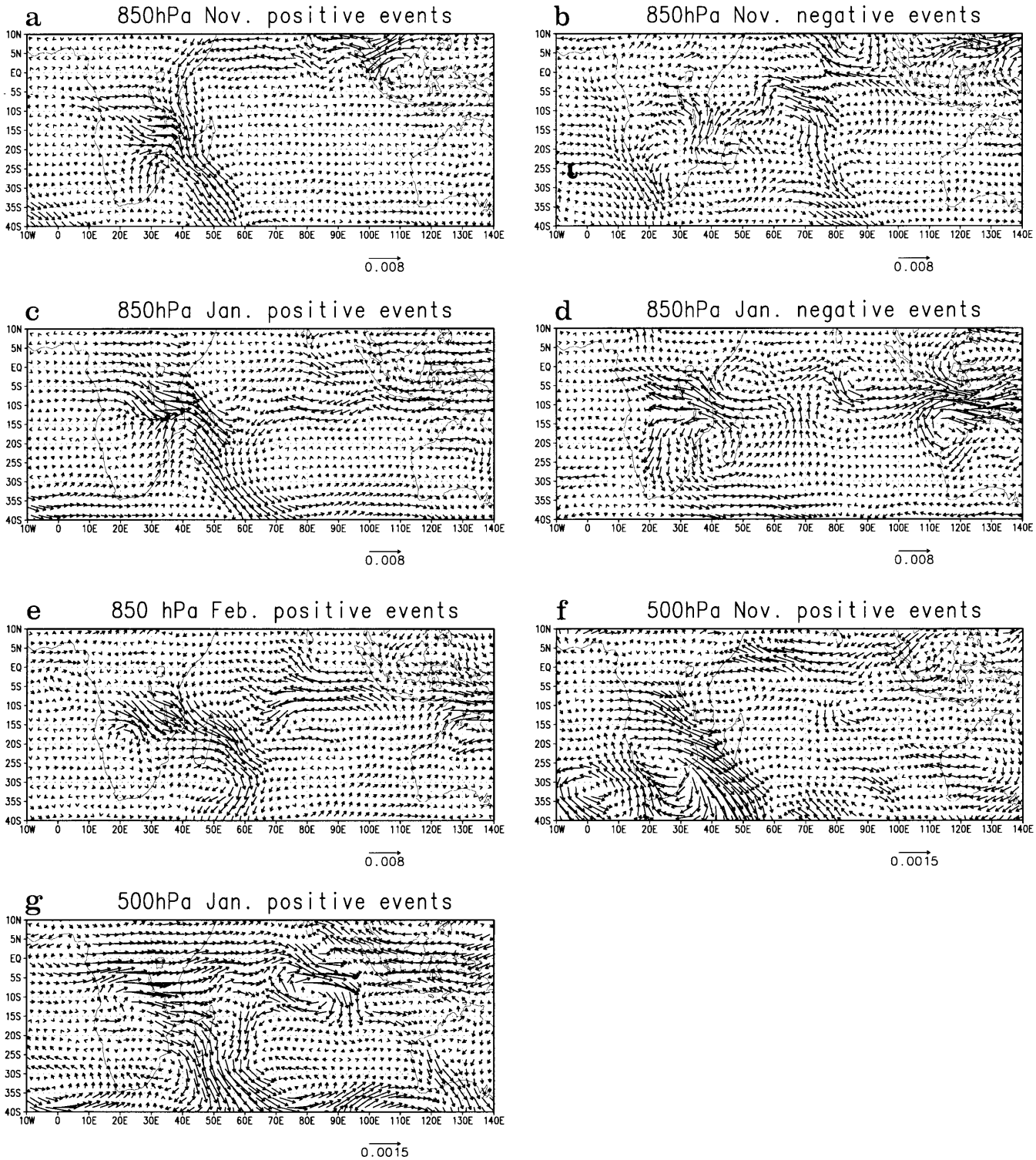


**Fig. 6a–g** Composite mean moisture flux anomalies (g $g^{-1}$ $ms^{-1}$) for **a** 850 hPa November positive events, **b** 850 hPa November negative events, **c** 850 hPa January positive events, **d** 850 hPa January negative events, **e** 850 hPa February positive events, **f** 500 hPa November positive events, **g** 500 hPa January positive events

45 °S 120 °E. At 200 hPa, a westerly trough overlies SA with a ridge southeast of Madagascar. As in early summer, this west-leaning system points to a baroclinic structure. In most respects, features of the January negative events are the opposite of those described for the positive events.

January low-level moisture flux composites (Fig. 6) for positive and negative events are similar to those

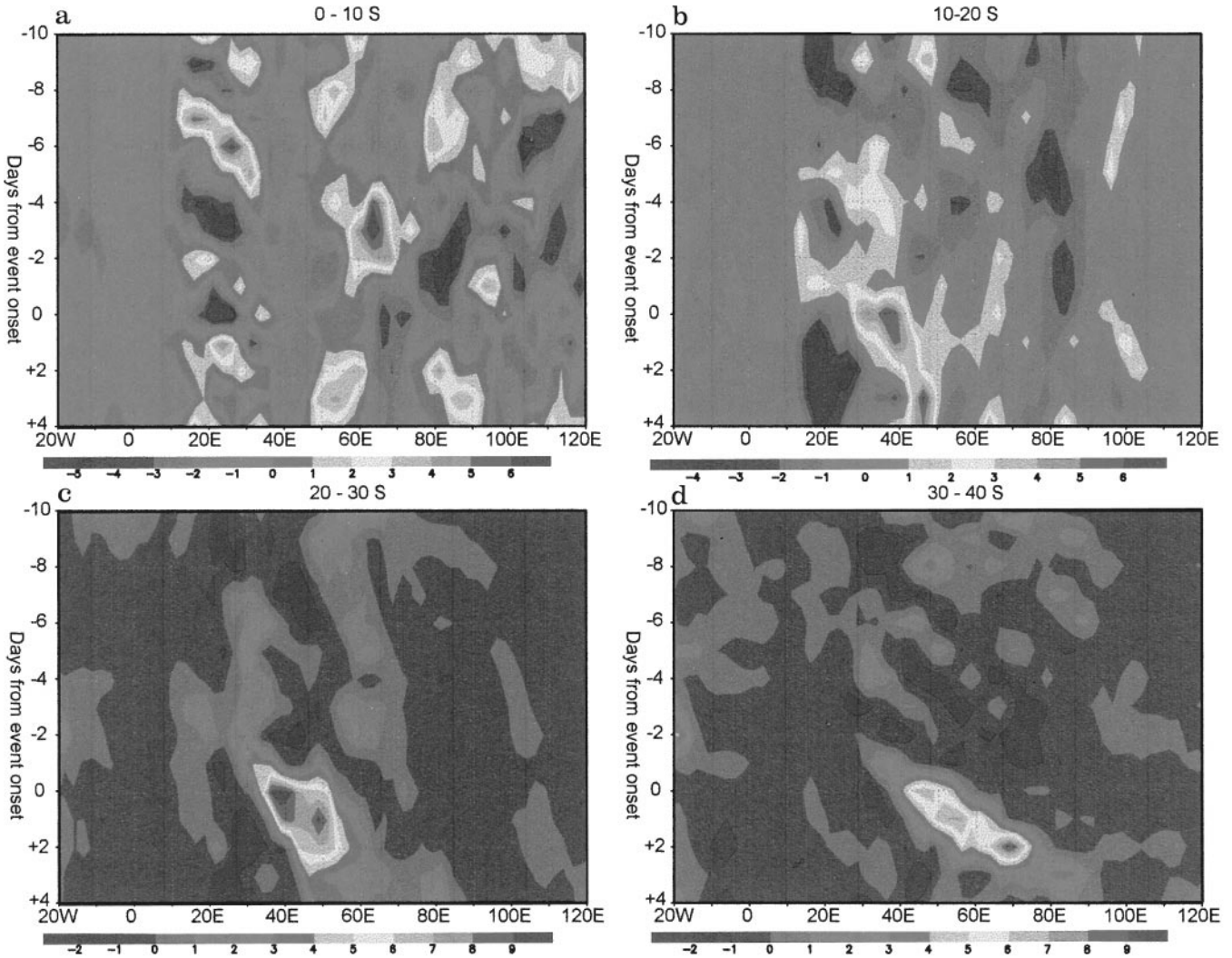


**Fig. 7a–d** Composite mean rainfall anomalies (mm day$^{-1}$) for periods preceding and following onset of November positive events averaged over latitudinal bands: **a** 0°–10 °S, **b** 10°–20 °S, **c** 20°–30 °S, **d** 30°–40 °S

for discussed for early summer. Important differences include the more southerly location of moisture flux across the Indian Ocean (centred on 10 °S) so that convergence of moisture from three sources occurs near 12 °S and 55 °E, somewhat further east than in early summer. Mid level (500 hPa) anomalous moisture flux (Fig. 6) for positive events in January are southward between 15 °S and 40 °S to the east of southern Africa. Anomalous westerly fluxes occur over most of equatorial Africa.

Time evolution of TTT episodes in January, revealed through Hovmoeller plots (Fig. 8) again show the pulsing of equatorial convection as well as convergence of tropical convection, though more so in the latitudinal slice centred on 15 °S. Eastward propagation of positive rainfall anomalies is clear in the band centred on 25 °S and 35 °S, less so along 15 °S.

As in the early summer, the zonally asymmetric circulation is dominated by wave 5 (Table 3) which accounts for over 60% of the variance in the 200 hPa anomalies at 45 °S. The amplitude of wave 5 in January is comparable to that found for November (36 gpm).

February near-surface circulation anomalies (Fig. 4) include the characteristic widespread anomalous surface low over the Mocambique Channel and much of the Indian Ocean. Unlike earlier months (notably January), the surface low extends over much of the African subcontinent, so that tropical convection over SA is linked with that over the SWIO, a distinguishing feature of February. Negative events are largely opposite to this (not shown). February moisture flux anomalies (Fig. 6) are similar to other months described here, except that the moisture source is confined to two regions, the Indian Ocean and equatorial Africa. The main convergence of moisture is east of Madagascar near 60 °E. The time evolution of TTT outbreaks in February is shown in Fig. 9. Pulsing in equatorial convection is clear along the band centred 5 °S 20 °E,

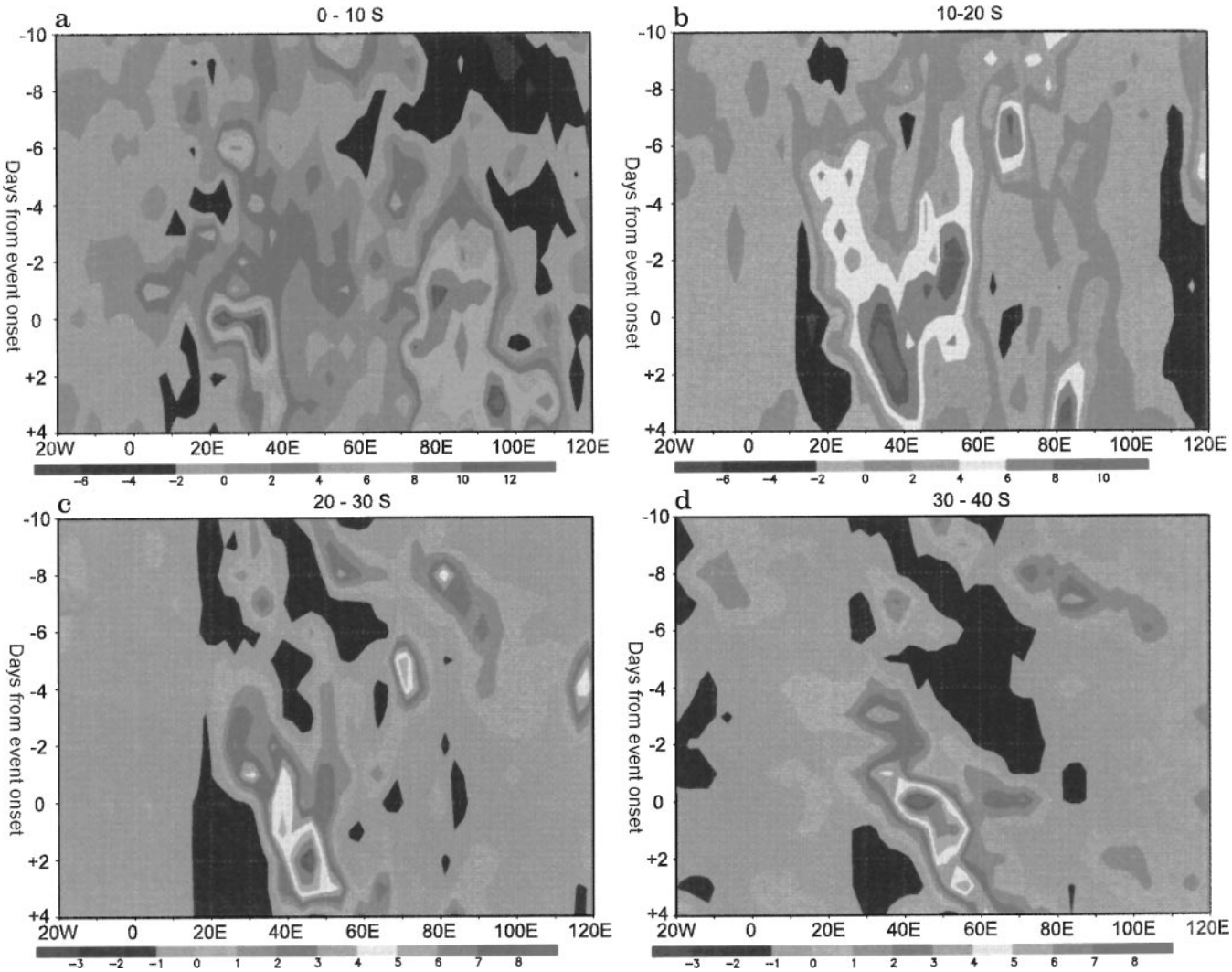


**Fig. 8a–d** Composite mean rainfall anomalies (mm day$^{-1}$) for periods preceding and following onset of January positive events averaged over latitudinal bands: **a** 0°–10 °S, **b** 10°–20 °S, **c** 20°–30 °S, **d** 30°–40 °S

although convergence from westward moving convection originating near 70 °E on the latitudinal band centred on 15 °S, while present, is weaker. Eastward propagation of the TTT associated rainfall is apparent along 25 °S and 35 °S.

Adjustments to the circulation associated with the generation of the unique distribution of February rainfall are reflected in the zonally asymmetric waves (Table 3) which show the importance of quasi-stationary waves 1, 2 and 3. This is the only summer month during which wave 5 is not important.

## 4 Structure of the global rainfall anomalies associated with tropical temperate troughs in SA and SWIO

Given the planetary scale of the anomalous moisture fluxes associated with major SA/SWIO TTT events an important question is whether these events are associated with characteristic patterns of global rainfall. Figure 10 presents mean RGPI rainfall anomalies for these composite events over the entire equatorial zone and Southern Hemisphere subtropics.

The spatial pattern of major rainfall anomalies (in the Southern Hemisphere convergence zones and the tropical Pacific region) for positive and negative events are almost opposites of each other in all months, adding confidence to a physical interpretation of the anomaly patterns. The rainfall dipole over the SA/SWIO region, coincident with the EOF loadings (Fig. 2), is immediately apparent, with rainfall anomalies in excess of 10 mm day$^{-1}$ and 5 mm day$^{-1}$ associated with positive and negative events respectively in each month. In November positive (negative) events are associated with markedly enhanced (suppressed) rainfall in the central equatorial Pacific (centred on the Dateline), the SACZ and equatorial Indian Ocean, with

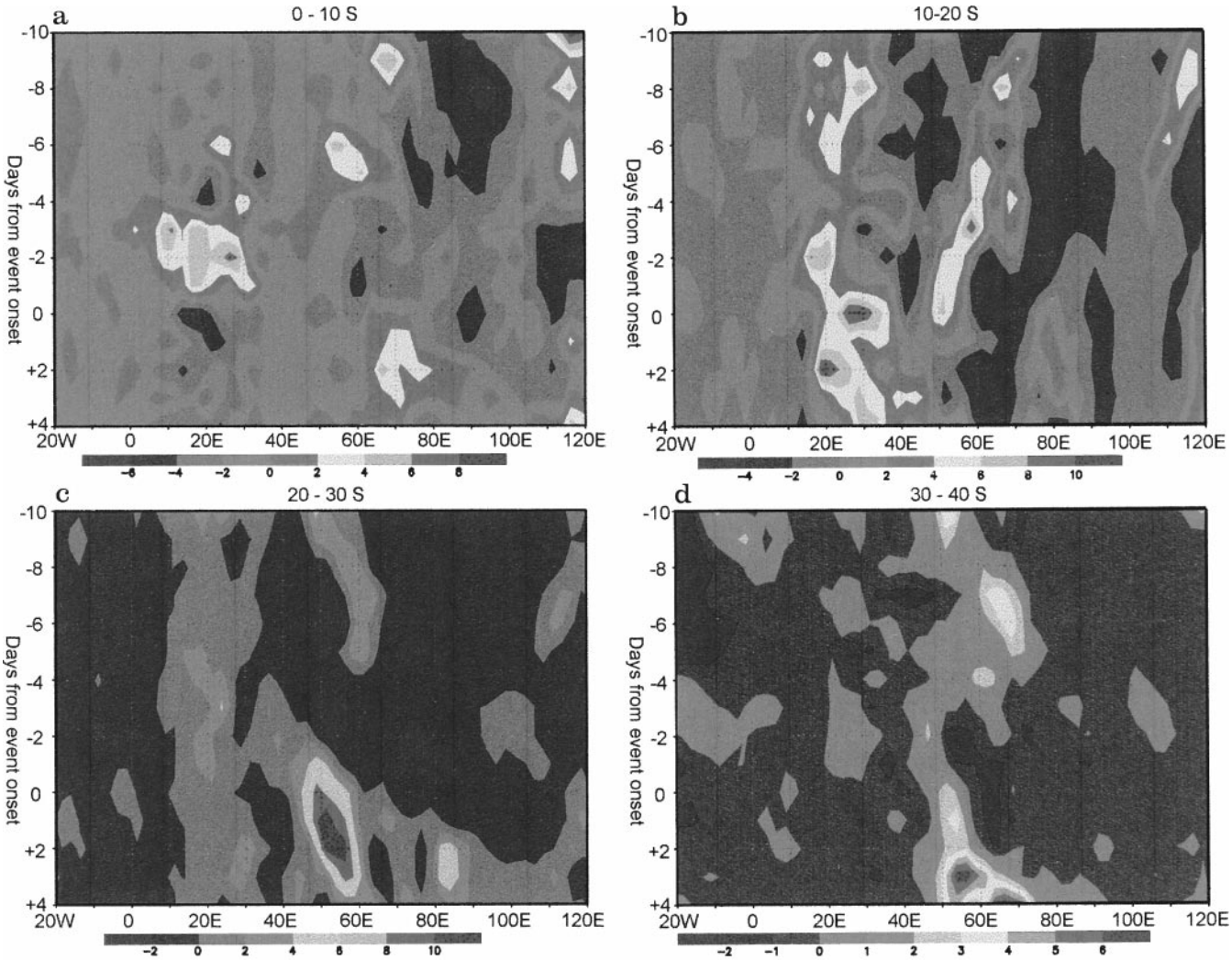


**Fig. 9a–d** Composite mean rainfall anomalies (mm day$^{-1}$) for periods preceding and following onset of February positive events averaged over latitudinal bands: **a** 0°–10 °S, **b** 10°–20 °S, **c** 20°–30 °S, **d** 30°–40 °S

suppressed (enhanced) rainfall over the Maritime Continent and equatorial west Africa. Along the SPCZ rainfall is enhanced (suppressed) in a band oriented northeast to southwest from 155 °W, 15 °S to 130 °W, 40 °S (Fig. 10a). Rainfall anomalies exceeding 5 mm day$^{-1}$ exist over extensive areas. A similar pattern of anomalies emerges in December (not shown).

In January the pattern is similar to that in November over equatorial Africa, much of the Maritime Continent and the SACZ. Rainfall anomalies in the SPCZ are displaced eastward, with enhanced (suppressed) rainfall associated with positive (negative) events centred on 165 °W, 5 °S, and extending from 140 °W, 15 °S to 120 °W, 40 °S (Fig. 10b). Substantially enhanced (suppressed) rainfall is apparent over the central and eastern Indian Ocean coincident with positive (negative) events.

It appears that associated with the phase of the SA/SWIO rainfall dipole, other dipole structures exist in certain key regions, for example the Maritime Continent/central Pacific, the SPCZ and to a lesser extent the SACZ. Comparison of Fig. 10 with global composite 200 hPa geopotential anomaly fields (Fig. 11) shows that statistically significant 200 hPa geopotential anomalies are generally in accord with rainfall anomaly patterns over the SPCZ and SACZ regions. Whilst we do not suggest any mechanisms for the observed pattern of rainfall anomalies in the tropical zone, the location of rainfall associated with tropical-temperate interaction along the SPCZ and SACZ in November–January may well relate to the longitudinal position of

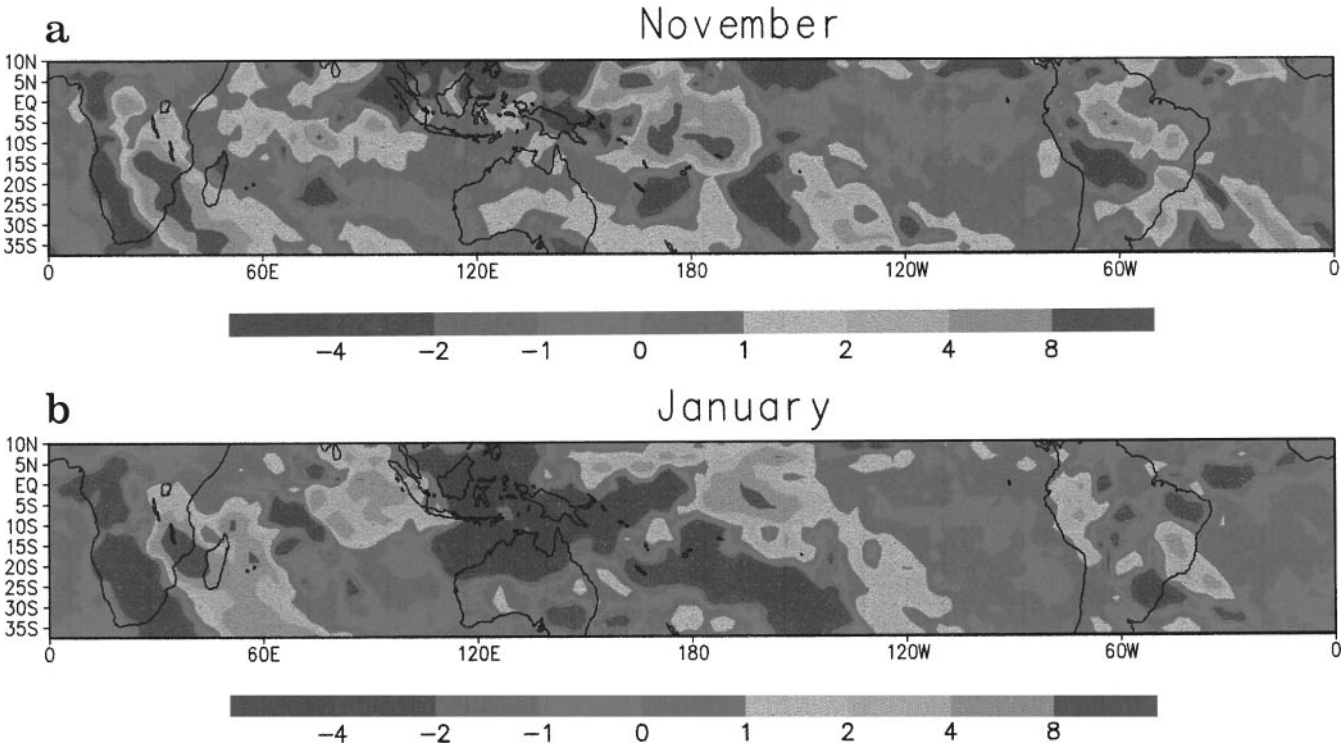


**Fig. 10a,b** Composite mean rainfall (mm day$^{-1}$) for positive minus negative events: **a** November, **b** January

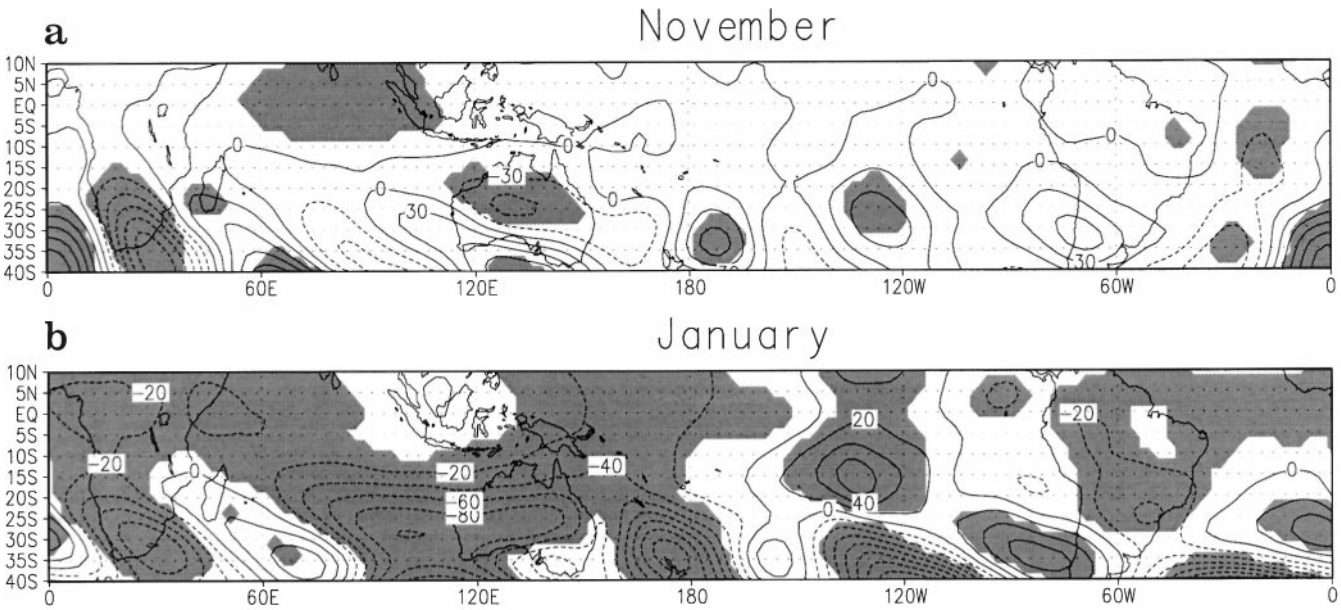


**Fig. 11a,b** Composite mean 200 hPa geopotential height (gpm) for positive minus negative events. **a** November, **b** January. *Shaded areas* are statistically significant at 95% level

the trough-ridge pattern of wave 5. The pattern of global tropical and subtropical rainfall anomalies in February, when waves 1, 2 and 3 dominate, is distinct in that positive events are associated with suppressed rainfall over the central and eastern Indian Ocean, enhanced rainfall over the western Pacific, and an incoherent pattern of anomalies in the SPCZ (not shown).

## 5 Discussion

### 5.1 Atmospheric circulation

Associations between rainfall anomalies over southern Africa and the modulation of atmospheric circulation have been extensively examined (Tyson 1981, 1983; Harrison 1984, 1986; Lindesay 1988; Jury 1992, 1996, 1997; Jury et al. 1992, D'Abreton and Lindesay 1993; D'Abreton and Tyson 1995; Mason and Jury 1997). Without exception, this work has used land-based rainfall indices as a sampling base for studying atmospheric circulation anomalies, usually on the basis of monthly averaged data. This study is novel in that a newly derived daily satellite rainfall data set allows an objective sampling base over both land and ocean which, together with the NCEP reanalysis data, provides a temporal and spatial resolution adequate to resolve specific synoptic conditions and the associated atmospheric circulation anomalies.

Tropical-temperate trough events are associated with a cyclonic circulation system in the vicinity of SA centred over the SWIO. From Fig. 4 it can be seen that positive (negative) events are associated with an eastward (westward) shift in the Indian Ocean and South Atlantic subtropical highs. The 200 hPa height anomaly fields of positive and negative events show a well-defined and opposing trough-ridge wave pattern in the midlatitudes poleward of 30 °S, with a wavelength of about 70° longitude. This is in line with the findings of Jury et al. (1992) that an alternation in a standing trough-ridge pattern with 70° longitude wavelength is associated with interannual rainfall variability over central South Africa. It appears, therefore, that the location of tropical temperate troughs and therefore the structure of moisture convergence and resulting rainfall in the SA/SWIO region, is strongly influenced by low frequency eddies in the midlatitudes.

The TTT features analysed here are clearly forced by a specific zonally asymmetric wave signature. Adjustments to the rainfall anomalies over southern Africa have previously have been assumed to be associated with the longitudinal position of the first ridge of wave 3 (Tyson 1981) which controls between 8 and 23% of the 500 hPa Southern Hemisphere variance at 45 °S (van Loon and Jenne 1972; Trenberth 1979). This analysis based on NCEP 200 hPa composite fields for daily rainfall events, point to Southern Hemisphere wave 5 as the most important feature in all months except February, when the quasi-stationary waves 1, 2 and 3 dominate. Streten (1973) and Yasunari (1977) suggest that waves 1 and 3 are most strongly linked to the major cloud bands of the Southern Hemisphere. However, the observed coherent dipole pattern of rainfall anomalies over the SPCZ and SACZ in phase with that over SA/SWIO suggests that wave 5 exerts a substantial influence on tropical-temperate interaction throughout the Southern Hemisphere.

### 5.2 Moisture transport

The southwest Indian Ocean is generally regarded as the source region of moisture for southern Africa (Taljaard 1986, 1987). This moisture is thought to be transported around the semi-permanent anticyclone off the east coast. Harrison (1986) has also drawn attention to the southward migration of tropical air from the ITCZ and Zaire air boundary. D'Abreton and Lindesay (1993) and D'Abreton and Tyson (1995) used land monthly rainfall over South Africa as a sampling base, and show evidence for a complex pattern of moisture transport with pronounced seasonal and interannual variability. During wet early summers moisture transport from Indian and Atlantic Oceans converges to the north of South Africa and is transported primarily by eddy divergence. Dry early summers are characterised by little or no transport from the Atlantic, but with an enhanced flux from the tropical Indian Ocean which is not transported southward to South Africa (D'Abreton and Tyson 1995). A major source of moisture in wet late summers is the western Indian Ocean north of Madagascar. Transport occurs southward in association with a thermally forced westerly wave while the eddy component of transport is minimal (D'Abreton and Tyson 1995).

Using COADS data, Rocha and Simmonds (1997) have also examined moisture flux on the basis of wet minus dry composites for seasons SON and DJF defined using rainfall in Southeast Africa. Wet minus dry SON composites resemble those shown for early summer months in this study, except that large flux anomalies fail to reach west of 70 °E whereas in our composites the path is much clearer.

Our findings are necessarily different from all previous studies since we are able to resolve the explicit rainfall episodes by using daily data. In addition we use both ocean and land-based rainfall in our EOF filtering scheme. We find that rainfall associated with tropical-temperate troughs over southern Africa and southwest Indian Ocean results from distinct patterns of anomalous low-level moisture transport which extend to the planetary scale, notably across the equatorial Indian Ocean. In early summer, these anomalies extend to at least 500 hPa over the Indian Ocean sector.

In all months, a broadly similar pattern of low-level moisture flux is produced. Positive events are associated with an anomalously strong easterly flux from the Indian Ocean and an anomalously strong westerly flux from central equatorial Africa, driven by a cyclonic circulation around the TTT system. These moist airstreams merge with the north easterly monsoon winds to produce convergence along the ITCZ and Zaire air boundary at about 20 °S. A northwesterly flux from this centre of convergence results along the TTT cloud band from east SA to the SWIO. The easterly flux extends across the entire Indian Ocean basin, with

reduced westerlies apparent over the Maritime continent in all months except February. The precise nature of this circulation pattern varies between months. During early and late summer, the magnitude of the westerly flow from equatorial Africa and the Atlantic is reduced such that the easterly flow dominates moisture transport. This is associated with the eastward movement of the Indian Ocean subtropical high during the peak summer months.

In contrast, during negative events in early summer the circulation over SA is dominated by a flow of north easterlies from the Indian Ocean entering the continent at around 10 °S (associated with the westward displacement of the Indian Ocean subtropical high) and a northwesterly flow around the temperate trough over the extreme southeast Atlantic. With weaker westerlies over the tropical zone moisture convergence (located over continental western SA) and poleward transport of moisture is much less than in positive events resulting in the observed weaker loadings in the rainfall EOFs. Negative events have a more localised circulation pattern, with no significant moisture flux anomalies over the Maritime Continent.

With the benefit of a daily satellite rainfall record as well as the NCEP Reanalysis data we can confirm the work of Harrison (1986) who argued that TTT systems represent a substantial transfer of moisture from the central Indian Ocean, eastern tropical Atlantic Ocean and central tropical Africa to SA and the SWIO. Low level moisture flux composite anomalies clearly show the poleward transport of moisture along the TTT cloud band located at the leading (easterly) edge of the temperate disturbance (Figs. 4–6), as suggested by Harrison (1986). This moisture convergence zone coincides with the loading pattern in the satellite-derived rainfall EOFs (Fig. 2), and the composite rainfall anomalies (Fig. 10). Driven by moisture convergence from the east and northeast Indian Ocean and equatorial Africa and the Atlantic, positive events result in greater rainfall and quite probably poleward transport of energy and momentum in comparison to negative events. What is particularly striking is that the synoptic scale features of TTTs in the study region are part of a large-scale circulation extending from the Maritime Continent in the east to the eastern Atlantic in the west, some 120° in longitude. The latitudinal extent of this circulation pattern is about 50°. The frequency of TTT occurrence however is such that the poleward meridonal component these events is not imposed on the mean moisture flux field.

The occurrence and location of TTT events appears closely tied to patterns of tropical convection over continental Africa and the Indian Ocean. Development of TTT events is associated with periodically enhanced convection in the latitude band 0°–10 °S, and intensification resulting from convergence of eastward and westward propagating convection in the band 0°–10 °S in early summer and 10°–20 °S in late summer. The TTT may provide the mechanism by which this enhanced convective energy and moisture is transported poleward.

## 6 Conclusions

Tropical-temperate trough systems are the dominant rain-producing synoptic type over the study region (Harrison 1986; Todd and Washington 1998; Washington and Todd 1999). This study is unique in that it is based on an objective definition of major TTT episodes (derived from recently developed daily satellite rainfall products), combined with recently released reanalysis products. This has enabled for the first time an objective description of the regional and global atmospheric circulation and moisture flux patterns associated with major TTT events, over an extended period.

In describing the patterns of atmospheric circulation, moisture flux, and rainfall, we have shown the significance of both tropical and extratropical dynamics, at the regional and planetary scales, in the development of TTT cloud bands. The results also highlight important intra-seasonal variations. Given that tropical SA represents the weakest of the three principle regions of Southern Hemisphere summer convection it has been suggested that this region is likely to be driven by one or both of the other major zones (Tyson 1986). We show that the most important region occurs east of South Africa, illustrating the need to consider the nature of rainfall dynamics of this region.

Tropical-temperate troughs are clearly of profound significance in the meridonal transfer of energy and momentum (Harrison 1986) and, on the basis of the results presented here, important future work should include a comprehensive analysis of momentum and ocean-atmosphere energy flux budgets in the region.

**Acknowledgements** The authors are grateful to the University of Oxford for support. The ISCCP satellite data were obtained from the NASA Langley Research Centre, EOSDIS, Distributed Active Archive Centre. NCEP reanalysis data were obtained from the National Centre for Atmospheric Research. We would also like to thank the anonymous referees for their constructive comments.

## References

Arkin PA, Meisner BN (1987) The relationship between large-scale convective rainfall and cold cloud over the western hemisphere during 1982–82. Mon Weather Rev 115: 51–74

Cohen AL, Tyson PD (1995) Sea-surface temperature fluctuations during the Holocene off the south coast of Africa: implications for terrestrial climate and rainfall. The Holocene 5: 304–312

D'Abreton PC, Lindesay JA (1993) Water vapour transport over southern Africa during wet and dry early and late summer months. Int J Climatol 13: 151–70

D'Abreton PC, Tyson PD (1995) Divergent and non-divergent water vapour transport over southern Africa during wet and dry conditions. Meteorol Atmos Phys 55:47–59

Harrison MSJ (1984) A generalized classification of South African summer rain-bearing synoptic systems. Int J Climatol 4:547–560

Harrison MSJ (1986) A synoptic climatology of South African rainfall variations. PhD Thesis, University of Witwatersrand, South Africa

Janowiak J (1988) An investigation of interannual rainfall variability in Africa. J Clim 1:240–255

Jury MR (1992) A climatic dipole governing the interannual variability of convection over the SW Indian Ocean and SE Africa region. Trends Geophys Res 1:165–72

Jury MR (1996) Regional teleconnection patterns associated with summer rainfall over South Africa, Namibia and Zimbabwe. Int J Climatol 16:135–53

Jury MR (1997) Inter-annual climate modes over southern Africa from satellite cloud OLR 1975–1994. Theor Appl Climatol 57:155–163

Jury MR, Pathack BMR, and Sohn BJ (1992) Spatial structure and interannual variability of summer convection over southern Africa and the SW Indian Ocean. S Afr J Sci 88:275–280

Kidd C, Adler RF (1997) Global satellite rainfall estimation: results of the third precipitation intercomparison project. Proc 23rd Conf Remote Sensing Soc Reading, UK. Remote Sensing Society, pp. 481–486

Kalnay E, Kanamitsu M, Kistler R, Collins W, Deaven D, Gandin L, Iredell M, Saha S, White,G, Woollen J, Zhu Y, Leetmaa A, Reynolds R, Chelliah M, Ebisuzaki W, Higgins W, Janowiak J, Mo KC, Ropelewski C, Wang CJ, Jenne R, Joseph D (1996) The NCEP/NCAR 40-year reanalysis project. Bull Am Meteorol Soc 77:437–471

Lindesay JA (1988) South African rainfall, the Southern Oscillation and a Southern Hemisphere semi-annual cycle. J Clim 8:17–30

Lindesay JA, Harrison MSJ, and Haffner MP (1986) The Southern Oscillation and South African rainfall. S Afr J Sci 8:196–198

Mason SJ, Jury MR (1997) Climatic change and inter-annual variability over Southern Africa: a reflection on underlying processes. Prog Phys Geog 21:24–50

Mo KC, Higgins RW (1996) Large-scale atmospheric moisture transport as evaluated in the NCEP/NCAR and NASA/DAO reanalyses. J Clim 9:1531–1545

Nicholson SE, Kim J (1997) The relationship of the El Niño- Southern Oscillation to African rainfall. Int J Climatol 17:117–136

North GR, Bell TL, Cahalan RF, Moeng FJ (1982) Sampling errors in the estimation of empirical orthogonal functions. Mon Weather Rev 110:699–706

Rocha A, Simmonds I (1997) Interannual variability of southeastern African summer rainfall, Part 1: relationships with air-sea interaction, Int J Climatol 17:235–266

Ropelewski CF, Halpert MS (1987) Global and regional scale precipitation patterns associated with El Niño/Southern Oscillation. Mon Weather Rev 115:1606–1626

Rossow WB, Schiffer RA (1991) ISCCP cloud data products. Bull Amer Meteorol Soc 72:2–20

Stokes SD, Thomas SG, Washington R (1997) Multiple episodes of aridity in southern Africa since the last inter-glacial Nature 38:154–158

Streten NA (1973) Some characteristics of satellite-observed bands of persistent cloudiness over the Southern Hemisphere. Mon Weather Rev 101:486–495

Taljaard JJ (1986) Change of rainfall distribution and circulation patterns over Southern Africa during in summer. J Clim 6: 579–592

Taljaard JJ (1987) The anomalous climate and weather systems over South Africa during summer 1975–1976. S Afr Weather Bur Tech Pap 16:80pp

Todd MC, Washington R (1998) Extreme daily rainfall in southern African and southwest Indian Ocean tropical-temperate links. S Afr J Sci 94:64–70

Todd MC, Washington R (1999) A simple method to retrieve 3-hourly global tropical and subtropical rainfall estimates from ISCCP D1 data. J Atmos Oceanic Technol 16:146–155

Trenberth KE (1979) Interannual variability of the 500 mb zonal mean flow in the southern hemisphere. Mon Weather Rev 107:1515–1524

Tyson PD (1981) Atmospheric circulation variations and the occurrence of extended wet and dry spells over southern Africa. J Clim 1:115–130

Tyson PD (1986) Climatic change and variability in southern Africa. Oxford University Press, Cape Town, SA

VandenHeever SC, Dabreton PC, Tyson PD (1997) Numerical simulation of tropical-temperate troughs over southern Africa using the CSU RAMS model. S Afr J Sci 93: 359–365

Van Loon H, Jenne RL (1972) The zonal harmonic standing waves in the Southern Hemisphere. J Geophys Res 77: 992–1003

Washington R, Todd MC (1999) Tropical temperate links in southern African and southwest Indian Ocean daily rainfall. Int J Climatol (in press)

Xie P, Arkin PA (1997) Global precipitation: a 17 year monthly analysis based on gauge observations satellite estimates and numerical model outputs. Bull Am Meteorol Soc 78: 2539–2558

Yasunari T (1977) Stationary waves in the Southern Hemisphere mid latitude zone revealed from average brightness charts. J Meteorol Soc J 55:274–285